Desalination and Water Treatment
www.deswater.com

doi: 10.5004/dwt.2021.27558

233 (2021) 106–117
September

Shrimp shells-derived biochar for efficient adsorption of Pb^{2+} in aqueous solutions

Tao Feng[a,b,*], Tan Yi[a], Qiaobing Wang[a], Pengwei Li[a]

[a]*College of Resources and Environmental Engineering, Wuhan University of Science and Technology, Wuhan 430081, China, Tel. +86 27 68862880; emails: fengtaowhu@163.com (T. Feng), 835286030@qq.com (T. Yi), 514348251@qq.com (Q. Wang), 826461375@qq.com (P. Li)*

[b]*Hubei Key Laboratory for Efficient Utilization and Agglomeration of Metallurgic Mineral Resources, Wuhan University of Science and Technology, Wuhan 430081, China*

Received 16 March 2021; Accepted 28 June 2021

ABSTRACT

Oxidation modification is an important technique for the development of novel adsorbents and has attracted considerable interest in recent years. A new and efficient Pb(II) adsorbent was developed in this study using simple and cost-effective protocols. Shrimp shell biochar (SSC) was obtained by pyrolysis of abandoned shrimp shells and subsequently treated with mixed acid to obtain modified biochar (SSC-M). The structure and adsorption properties of SSC and SSC-M were investigated for Pb(II) adsorption using a variety of characterisation methods. Both SSC and SSC-M exhibited excellent aqueous Pb(II) adsorption capacities and achieved maximum adsorption capacities of 94.16 and 156.48 mg g^{-1} at the optimal condition, respectively. The adsorption of lead ions by SSC and SSC-M followed a pseudo-second-order kinetics model and a monolayer adsorption process. Moreover, the prominent adsorption performance of SSC-M for Pb(II) was mainly attributed to electrostatic interactions and surface complexation. SSC-M can be a promising and affordable adsorbent for Pb(II) ions owing to its significant adsorption capacity.

Keywords: Shrimp shell; Biochar; Oxygen functional; Adsorption performance; Lead removal

1. Introduction

Heavy metal pollution results from heavy metals and their compounds, which are easily produced by exhaust gas emissions, mining, wastewater irrigation, and other man-made factors. Heavy metal pollution is different from organic pollution because some organic pollutants can be reduced or alleviated by physicochemical or biological treatments in nature [1]. However, heavy metals cannot be biodegraded and have high toxicity and enrichment; they not only damage the environment but are also health hazards for human beings even at low concentrations. Among them, lead has been identified as a major human health hazard because it is harmful to the central nervous and reproductive systems [2]. According to the Ministry of Health of the People's Republic of China, the permissible level of Pb(II) in drinking water is 0.01 mg L^{-1} [3]. Therefore, the removal and elimination of lead from contaminated water and wastewater are necessary for the protection of the environment and human health.

Many studies have adopted various techniques to remove Pb from contaminated water, such as chemical precipitation, ion exchange, membrane separation and adsorption. Among them, adsorption has attracted universal attention for its unique characteristics, such as simple operation, low energy consumption, and high resource availability. To date, various adsorbents have been widely studied to remove Pb from wastewater, including activated

* Corresponding author.

carbon, graphene, and bio-adsorbents. Biochar has been widely applied to remove aqueous contaminants owing to its high surface area, large adsorption capability, and different oxygen functional groups [4–7].

The physicochemical properties of biochar are largely determined by the number and properties of its surface functional groups. Carbon adsorbents are often modified to further improve their adsorption capability. Modifying biochar can change its physical and chemical properties and greatly improve its pollutant adsorption efficiency [8–12]. Moreover, oxidation modifications are a common method of creating oxygen-containing functional groups (such as –OH, COOH, –C=O, and –C–O) on biochar surfaces [13]. In general, oxidation modification is carried out in the presence of inorganic acids and oxidants, and this acid treatment is beneficial for enhancing the adsorption capacity of biochar with respect to metal ions.

In addition, the adsorption of metal ions with biochar correlates to its raw material [14,15]. Shrimp shells are rich in $CaCO_3$, chitin, protein, and other nitrogen-containing substances and can be converted into porous carbon materials by a high-temperature carbonisation process, which can be utilised to absorb pollutants in water [16–18]. Moreover, 6–8 million tons of discarded shrimp shells are annually produced due to the global consumption of shrimp, from which ~1.5 million tons of shell wastes are generated from Asia alone [19]. In most developing economies, waste shrimp shells are usually buried in landfills or dumped into the sea directly. Such wastes can result in severe environmental pollution by creating health hazards and undesirable odours. Therefore, to save resources and protect the environment, it is necessary to efficiently reuse waste shrimp shells. Currently, there are a few studies on the removal of contaminants from water by shrimp shells or shrimp shell-derived materials. He et al. [20] synthesised a shrimp shell-based hydrochar adsorbent which demonstrated a long aliphatic chain structure with rich nitrogen-containing functional groups (e.g., 27.25% of –HN–C=O and 53.60% of $–NH_2$). The adsorption of methyl orange followed a pseudo-second-order kinetics model; it was a monolayer adsorption process with a maximum adsorption capacity of 755.08 mg g^{-1}. Qin et al. [21] converted shrimp shells into novel N-doped hierarchically porous carbons, which were used to effectively eliminate sulfamethazine (SMZ) and chloramphenicol (CAP) from water. The results showed that adsorption processes were governed predominantly by intraparticle diffusion and film diffusion, and the maximum monolayer adsorption capacity for SMZ and CAP was 699.3 and 742.4 mg g^{-1}, respectively. Park et al. [22] investigate the characteristics of crawfish char (CFC) derived at different pyrolysis temperatures and evaluate its adsorption characteristics on phosphate. Maximum adsorption capacities of phosphate by CFC at different pyrolysis temperatures were high in order of CFC800 (70.9 mg g^{-1}) > CFC600 (56.8 mg g^{-1}) > CFC400 (47.2 mg g^{-1}) >> CFC200 (9.5 mg g^{-1}) ≈ uncharred crawfish feedstock (7.1 mg g^{-1}). Further, the adsorption characteristics of shrimp shells or shrimp shell-derived materials in an aqueous solution were preliminarily studied in the above research. However, the adsorption mechanism of shrimp shell-based biochar with respect to Pb(II) was not analysed in depth.

In the present study, mixed acid was used to modify biochar from shrimp shells; the feasibility of adsorbing Pb(II) from water using raw shrimp shell biochar (SSC) and mixed-acid-modified biochar (SSC-M) were investigated and compared; the effects of solution pH, adsorption time, and initial metal ion concentration on adsorption capacity of the adsorbent were investigated; the mechanism of lead adsorption by SSC-M was explored.

2. Experimental

2.1. Materials

All chemicals and reagents used in this study were analytically pure. Sodium hydrate, sodium nitrate, and nitric acid were purchased from Sinopharm Chemical Reagent Co., Ltd., (China). Hydrochloric acid was obtained from Xinyang Chemical Reagent Factory, (China). Lead nitrate was obtained from China Pharmaceutical Shanghai Chemical Reagent Co., Ltd., (China).

2.2. Biochar preparation and modification

Shrimp shells (SS) were washed and subsequently dried at 60°C–80°C for 4–8 h; thereafter, the feedstock was ground and sifted to a uniform size of 0.15–0.20 mm. To prepare raw biochar (SSC), SS powder was heated to 800°C at 10°C/min in a tubular furnace (SK-GO5123K, Tianjin Zhonghuan Electric Furnace, China) and kept for 2 h under a nitrogen atmosphere with a nitrogen flow rate of 100 mL/min. After naturally cooling to ambient temperature, the product was reacted thoroughly with 5% HCl to completely remove $CaCO_3$ and rinsed with distilled water several times to ensure a neutral pH. Finally, the product was dried for 10 h in an oven at 90°C–110°C to obtain raw biochar.

Modified biochar was prepared by the condensation reflux method: (1) SSC was added to boiling water for 30 min; SSC was dried for 4 h after filtration; (2) 5 g of dried material was mixed with 40 mL of mixed acid (with a 1:3 volume ratio of HNO_3/H_2SO_4) in a round-bottom flask; the mixture was placed in a water bath at 60°C for 4 h and rinsed with distilled water several times to ensure neutral pH; (3) the washed material was dried at 120°C for 8 h to obtain modified biochar (SSC-M).

2.3. Batch adsorption experiments

Batch adsorption experiments were conducted to determine the Pb(II) adsorption capacities of the two biochars. In this regard, 0.1 g of biochar was loaded into a 250 mL Erlenmeyer flask containing 100 mL of lead nitrate solutions with a concentration of 200 mg L^{-1}. The initial pH was adjusted between 2.0 and 6.0 by adding 2 M HCl or NaOH. The Erlenmeyer flasks were shaken at 180 rpm and 25°C ± 0.5°C in a temperature-controlled shaker until adsorption equilibrium was achieved. Subsequently, the mixture was filtered through a 0.6 μm membrane. Pb(II) concentration in the filtrates was measured using an atomic absorption spectrophotometer (novAA350, Jena Analytical Instruments GMBH, Germany). The adsorption performance of the two biochars was compared based on the

decrease in the Pb(II) amount in the solution. The adsorption capacity at equilibrium was calculated according to Eq. (1):

$$Q_e = \frac{\left(C_0 - C_e\right)}{m} \times V \tag{1}$$

where Q_e (mg g^{-1}) is the amount adsorbed at equilibrium; V (mL) is the solution volume; m (g) is adsorbent mass; C_0 (mg L^{-1}) and C_e (mg L^{-1}) are the initial and equilibrium concentrations of Pb(II), respectively.

2.4. Adsorption isotherm

To examine the adsorption isotherm of SSC and SSC-M, 0.1 g adsorbent was added to 100 mL Pb(II) solutions with different initial concentrations (5–300 mg L^{-1}). The experimental data were calculated to determine the adsorption isotherm by using the Freundlich and Langmuir models, as introduced in the following equations.

$$\text{Langmuir model: } q_e = \frac{q_m b C_e}{1 + bC_e} \tag{2}$$

where q_e is the equilibrium adsorption capacity (mg g^{-1}); C_e is the concentration in solution at equilibrium (mg L^{-1}); q_m (mg g^{-1}) is defined as the maximum adsorption amount; b (L mg^{-1}) denotes the binding sites for Pb(II).

$$\text{Freundlich model: } q_e = K_F C_e^{\frac{1}{n}} \tag{3}$$

Both K_F (mg L^{-1}) and $1/n$ are the characteristic adsorption amount and intensity of biochar, respectively.

A model is considered as good if the correlation coefficient (R^2) is high, and all statistical errors and standard deviation (SD) are minimum. The SD and the statistical errors as the residual sum of square error (RSSE) and the root mean square error (RMSE) are calculated according to Eqs. (4)–(6) as follows:

$$\text{SD} = \sqrt{\frac{\sum\left\{\left(q_{\text{exp}} - q_{\text{cal}}\right)/q_{\text{exp}}\right\}^2}{N-1}} \tag{4}$$

$$\text{RSSE} = \sum_{i=1}^{N}\left(q_{\text{exp}} - q_{\text{cal}}\right)^2 \tag{5}$$

$$\text{RMSE} = \sqrt{N\sum_{i=1}^{N}\left[\frac{\left(q_{\text{exp}} - q_{\text{cal}}\right)^2}{N}\right]} \tag{6}$$

where q_{exp} and q_{cal} are the amounts of Pb(II) adsorbed experimentally and calculated from the model, respectively, N is the number of experimental data points, and i is the number of parameters in the model.

2.5. Adsorption kinetics

In this experiment, 0.1 g biochar was loaded into 100 mL Pb(II) solution with a concentration of 200 mg L^{-1} at ambient temperature. The residual Pb(II) content at different time intervals (10, 20, 30, 60, 120, 180, and 300 min) was analysed to determine the adsorption kinetics. The pseudo-first-order equation (Lagergren equation) can be defined as:

$$q_t = q_e\left(1 - e^{-k_1 t}\right) \tag{7}$$

where q_t is the amount of Pb(II) sorbed at time t (mg g^{-1}), q_e is its value at equilibrium (mg g^{-1}), and k_1 is the rate constant of the pseudo-first-order process (min^{-1}).

The pseudo-second-order model can be defined as:

$$\frac{t}{q_t} = \frac{1}{k_2 q_e^2} + \frac{t}{q_e} \tag{8}$$

where k_2 is the rate constant of the pseudo-second-order process (g mg^{-1} min) and q_t and q_e have the same meaning as in the pseudo-first-order equation.

2.6. Characterization

The specific surface area and pore volume of biochars were investigated by the Brunauer–Emmett–Teller (BET; Micromeritics, USA) method using an ASAP-2046 analyser, based on the N_2 adsorption/desorption isotherm data. The physiochemical material properties were imaged using a scanning electron microscope (SEM; Hitachi, Japan) with energy-dispersive X-ray spectroscopy (EDS). X-ray photoelectron spectroscopy (XPS, Thermo Fisher, USA) was also used to obtain information on surface chemistry. The surface functional groups were characterized by Fourier-transform infrared spectroscopy (FTIR; Thermo, USA). Powder X-ray diffraction (XRD; PANalytical B.V., Netherlands) patterns were recorded on a D/MAX-III type A fully automatic X-ray diffractometer with Cu Kα radiation.

3. Results and discussion

3.1. Characterization

The surface micro-morphologies and chemical compositions of SSC and SSC-M determined by SEM-EDS analysis are shown in Fig. 1. The surface of both materials is composed of irregular layer-like structures that provide strength, toughness, and a large surface area for adsorption. Unlike the smooth surface of SSC (Fig. 1A), the surface of SSC-M is evenly covered with small particles. The original surface texture and porosity are destroyed after functionalisation with the mixed acid solution. This is because mixed acid modification can erode biochar surface; the mixed acid removes $CaCO_3$ that exists in the SSC surface aperture tunnels leading to the collapse of some large pores, and the pore structure of the shrimp shell biochar readjusts to form smaller pores. EDS data shows that the Pb content in SSC-M increases significantly after adsorption, indicating the adsorption of Pb(II) onto the surfaces of the modified biochar.

The N_2 adsorption–desorption isotherms of SSC and SSC-M are shown in Fig. 2. The BET specific surface areas and porous structure parameters are summarised in

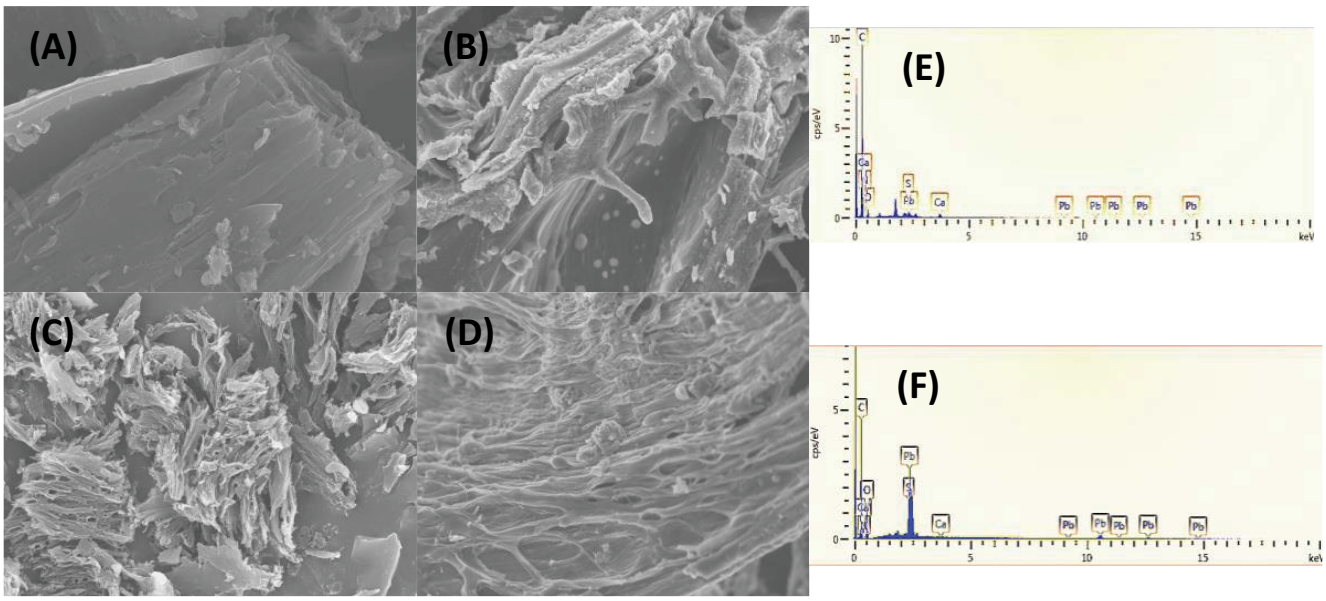

Fig. 1. SEM-EDS analysis of (A) SSC before adsorption, (B) SSC-O before adsorption, (C, E) SSC after adsorption and (D, F) SSC-O after adsorption.

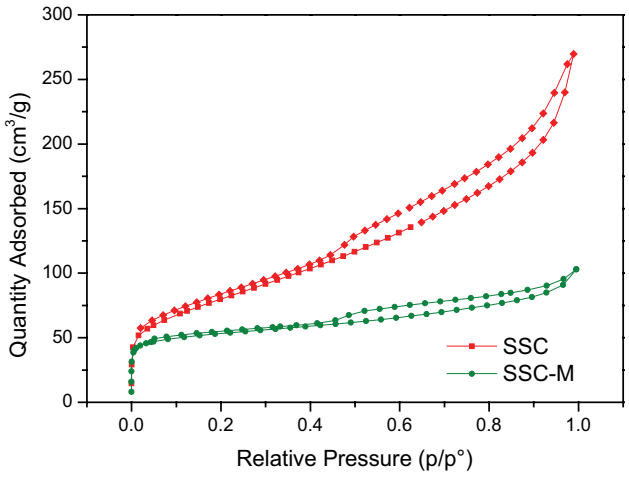

Fig. 2. N_2 adsorption–desorption isotherm for SSC and SSC-M.

Table 1. The adsorption isotherms of SSC and SSC-M satisfy the type IV description with the type H_1 hysteresis loops in the IUPAC classification, representing a typical mesoporous structure [23]. Moreover, the isotherms change in a relatively narrow range of pressures, which further indicates that the pore size distribution of the material is uniform and that the pore structure is regular [24,25]. After modification, the specific surface area of biochar decreases from 291.3 to 178.14 $m^2\ g^{-1}$. The average pore-size of SSC and SSC-M was found to be 5.73 and 31.9 nm, respectively. The surface of biochar was eroded under the action of strong acid, resulting in the collapse of the surface pores and the destruction of the original pore structure. And the oxygen-containing functional groups were loaded onto the lamellar/aperture structures, which may explain the relative reduction in surface area and the increase in pore size [6]. Fig. 2 also shows that SSC-M adsorbs lower volumes of nitrogen compared to SSC. This result tallies with the decrease in pore volume of the biochar resulting from the incorporation of oxygen-containing functional groups. In summary, the well-developed mesoporous structure, relatively high surface area, and large pore width of SSC-M are probably superior to those of SSC for the diffusion of pollutants into the inner pore system of the sorbents and the subsequent adsorption removal.

The functional groups in biochar are closely related to its physical and chemical properties and can indicate its adsorption capacity. To probe the effect of modification on the functional groups of biochar, FTIR analysis are conducted and the resulting spectra are shown in Fig. 5. Evidently, the vibrational absorption peaks at 3,406 and 1,384 cm^{-1} are related to the stretching vibration of O–H [26,27]. The peaks at 2,922 and 2,847 cm^{-1} represent

Table 1
Physicochemical properties (before adsorption) and elemental composition (after adsorption) of SSC/SSC-M

Adsorbent	S_{BET} ($m^2\ g^{-1}$)	Pore diameter (nm)	Pore volume ($cm^3\ g^{-1}$)	Elemental composition (%)				
				C	O	Pb	Ca	S
SSC	291.3	5.73	0.42	82.75	13.23	2.57	1.19	0.26
SSC-M	178.14	31.9	0.16	53.14	26.90	19.81	0.16	0

stretching vibrations of C–H on saturated carbon [28]. As depicted in Fig. 3A and C, the peaks at 1,717 cm^{-1} can be ascribed to the stretching vibration of carbonyl groups; this characteristic peak does not exist in SSC. This indicates that the carboxyl group is loaded onto the surface of biochar after mixed acid modification. These three vibration peaks (3,406; 2,922 and 2,847 cm^{-1}) are obviously enhanced in Fig. 5A, compared to those in Fig. 5B, indicating that the strength and quantity of carboxyl and hydroxyl groups increase in SSC-M. The peak at 1,599 cm^{-1} resulted from C=C or the skeleton vibrations of the aromatic ring, and it shifts slightly to 1,587 cm^{-1} in Fig. 6C–D [29]. The peaks at 1,093 and 791 cm^{-1} can be assigned to aliphatic ether and aromatic C–H banding, respectively.

XPS analysis was further performed to investigate the chemical state and surface composition of the biochars. The survey spectra indicated no obvious impurities in SSC and SSC-M [30]. Fig. 4B shows a stronger O 1s peak in the spectrum after modification, which confirms that mixed-acid-modification can successfully add O to biochar. As shown in Fig. 4B and C, high-resolution spectrum of C 1s spectrum of SSC can be divided into three peaks that can be assigned to sp3 (C–C, 284.8 eV), bonded carbon (C–O, 286.3 eV), and carbonyl groups (C=O, 289 eV) [31]. A similar result is observed in the deconvolution of C 1s spectrum of SSC-M, which implies that the modification may not have a remarkable effect on these C-containing functional groups. The O 1s spectra of SSC and SSC-M (Fig. 4E and F) show 2 peaks in the O 1s for both SSC and SSC-M: –OH at 531.35/531.65 eV and C–O at 532.45/532.75 eV. The content of C–O and C=O increases after modification, from 19.7% to 21.6% and from 13.3% to 15.8%, respectively (as shown in Table 2). This indicates that modification increases the number of carboxyl groups and ether bonds on the biochar surface, in accordance with the FTIR analysis mentioned earlier.

The XRD patterns of SSC and SSC-M are compiled in Fig. 5. Both Fig. 5A and B show large envelope peaks indicating amorphous structures. As shown in Fig. 5A, SSC exhibits a relatively obvious diffraction peak at around 19° which belongs to the chitin class. However,

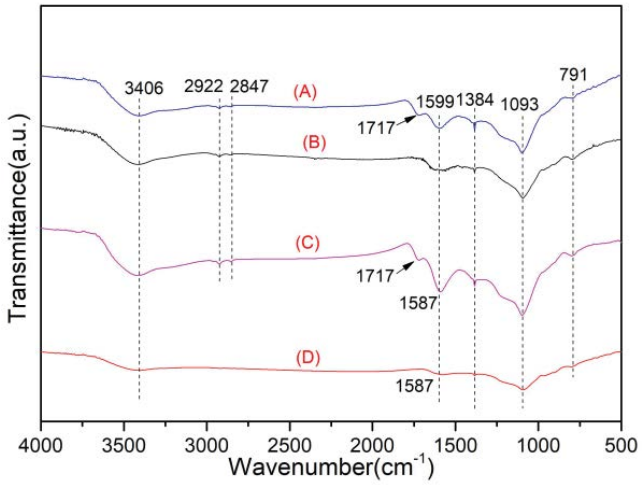

Fig. 3. FTIR spectra of (A) SSC-M before adsorption, (B) SSC before adsorption, (C) SSC-M after adsorption and (D) SSC after adsorption.

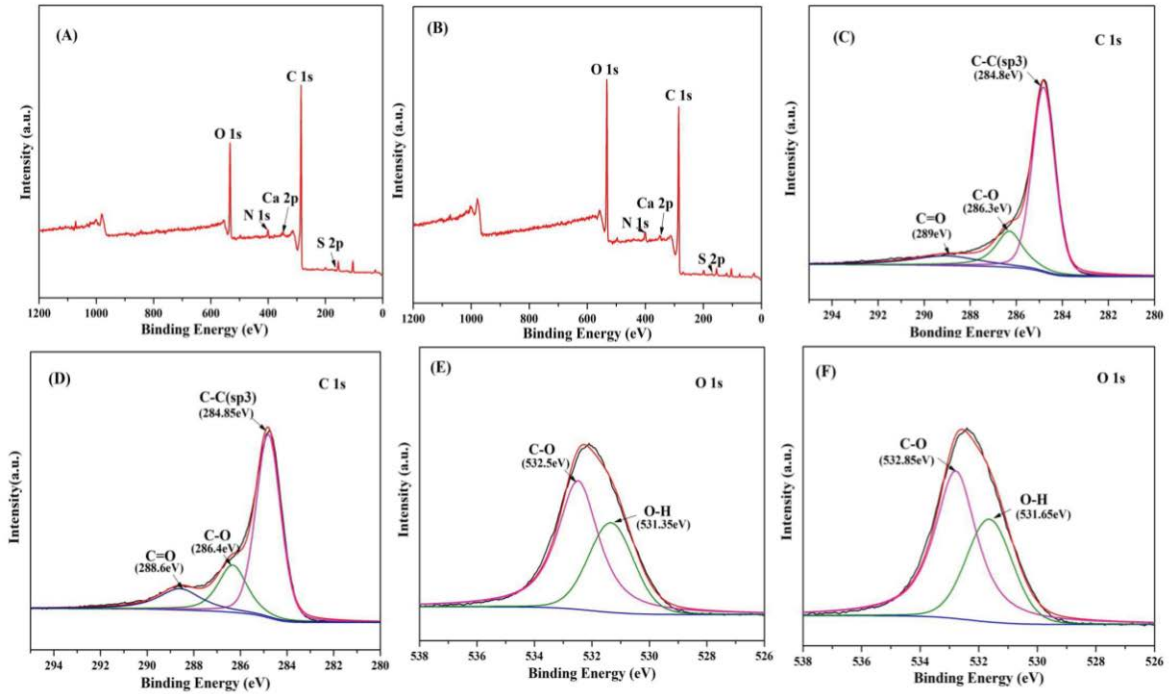

Fig. 4. XPS scan spectra of SSC and SSC-M before adsorption: wide scan for (A) SSC and (B) SSC-M, deconvolution of C 1s spectrum for (C) SSC and (D) SSC-M and deconvolution of O 1s spectrum for (E) SSC and (F) SSC-M.

after modification, the diffraction peaks of the original chitin decrease or disappear as shown in Fig. 5B; this is because the mixed acid can corrode the surface structure of biochar and destroy the original crystal structure. This indicates that the mixed acid modification has a fundamental effect on the surface structure and chemical properties of biochar. The diffraction peaks in Fig. 5C shifted slightly to a larger 2θ compared to those in Fig. 5B; the intensities noticeably decrease, suggesting that chemical reactions took place during adsorption, which is consistent with the results of the adsorption kinetic analysis. After adsorption, the ordered structure of SSC-M disappears, which destroys the molecular crystal structure and decreases the crystallinity; this leads to the migration of the diffraction peaks or the weakening of the intensities.

3.2. Adsorption performance

3.2.1. Effect of pH

The pH of the solution significantly affects the adsorption efficiency, which can influence the ion form of Pb, surface charge, and binding sites of biochar [32,33]. To identify the optimal solution pH for the studied biochar as an adsorbent, Pb(II) adsorption was measured using solutions with pH values ranging from 2 to 6 (Fig. 6). As shown in Fig. 6A, the SSC and SSC-M adsorption capacity for Pb(II) at a pH of 2 is very low. With increasing pH, the adsorption capacity of the biochars gradually increases. The adsorption capacity of biochar for Pb(II) slightly decreases at a pH > 5. Consequently, a solution pH of 5 was chosen for subsequent experiments.

The effect of pH on the adsorption process can be attributed to the competition between H^+ and Pd(II). In the case of low pH, a large number of available H^+ ions occupy the adsorption sites of the biochar functional

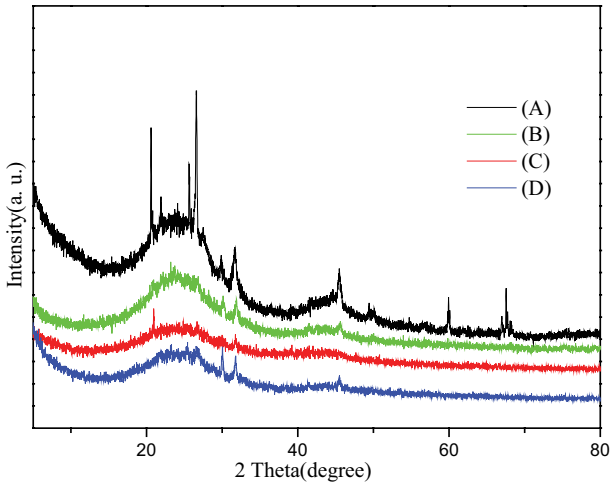

Fig. 5. Powder XRD patterns: (A) SSC before adsorption, (B) SSC-M before adsorption, (C) SSC-M after adsorption and (D) SSC after adsorption.

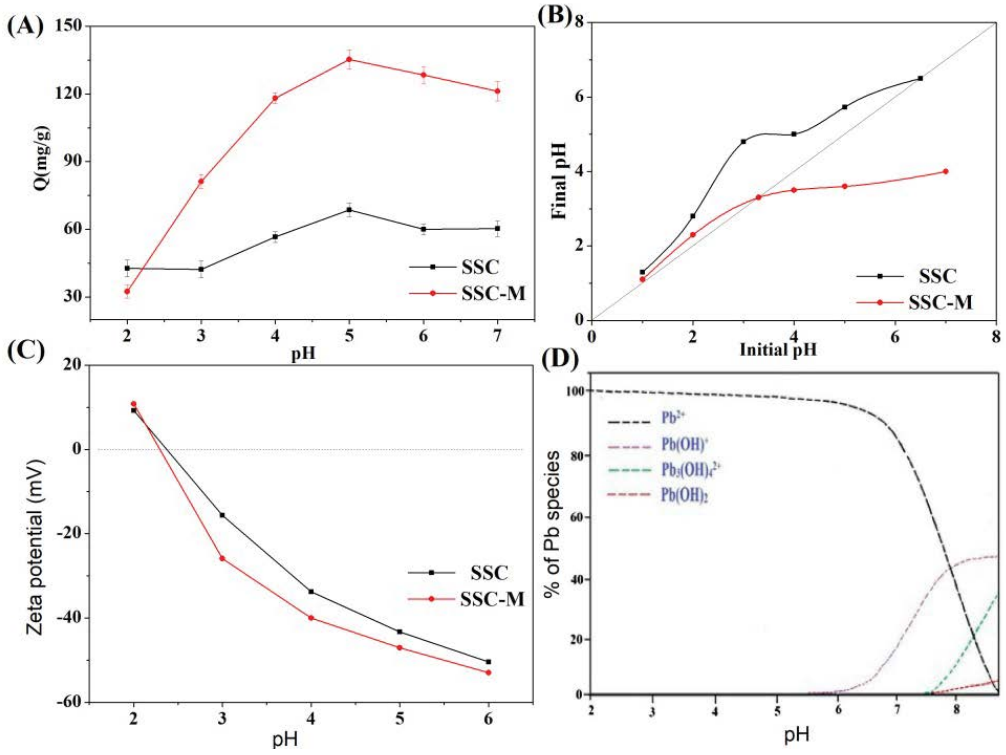

Fig. 6. (A) Effect of pH on adsorption of Pb(II) on SSC and SSC-M, where C_0[Pb(II)] = 200 mg L^{-1}; m/V = 1 g L^{-1}; t = 120 min; T = 25°C ± 0.5°C, (B) changes in after Pb(II) adsorption by SSC and SSC-M, (C) zeta potential of SSC and SSC-M and (D) lead species in aqueous solution as a function of pH [24].

Table 2
XPS results from O 1s spectra and C 1s spectra

Peak	SSC		SSC-M	
	Position (eV)	%	Position (eV)	%
C–C	284.9	67	284.8	62.6
C–O/C–O–C	286.3	19.7	286.4	21.6
C=O	288.3	13.3	288.6	15.8

groups, which hinders the binding of Pb(II) to those functional groups. With an increase in pH, the deprotonation of the functional groups on the biochar surface increases, and hence, Pb(II) ions combine with the biochar by electrostatic interaction. It was noticed that Pb^{2+} is the predominant species at low pH (nearly less than pH 6). At pH from 6 to 7.5, a mixture of Pb^{2+} and $Pb(OH)^{+}$ are present, as shown in Fig. 6D. While at pH higher than 5.0, the decreasing trend was caused by the formation of soluble hydroxyl complexes.

pH_{PZC} is related to the adsorption phenomenon. When the number of positive and negative charges on the biochar surface are equal, the zeta potential of biochar is zero, during which the pH of the solution is pH_{PZC} [34]. The pH_{PZC} values of SSC and SSC-M are approximately 2.37 and 2.29, respectively, as shown in Fig. 6C. This means that the surface charge becomes positive at a pH < pH_{PZC} and negative at a pH > pH_{PZC}. If the solution pH is lower than pH_{PZC}, the active sites on the adsorbent surface become inactive for Pb ion adsorption because the adsorbent surface is protonated. However, increasing the pH decreases the protonation of the functional groups on the adsorbent surface and thus enhances Pb(II) adsorption via electrostatic attractions.

3.2.2. Effect of initial Pb(II) concentration

Concentration difference is a driving force in mass transfer operations [35]. The uptake of Pb(II) by SSC and SSC-M was investigated over a concentration range of 50–300 mg L^{-1} at a pH of 5. Fig. 7A shows the equilibrium adsorption amount on the basis of equilibrium Pb concentrations and the related isotherm fitting. Increasing the initial concentration of Pb(II) leads to a decrease in its removal percentage. This can be attributed to the fact that at low concentrations, a high proportion of active sites is available on the adsorbent surface for the adsorption of metal ions. However, at high concentrations (>100 mg L^{-1}), the active surface sites on the adsorbents are saturated by the adsorbate, leading to a decrease in the adsorption percentage of Pb(II) [32,36]. In addition, the amount of Pb(II) adsorbed by SSC-M is greater than that of SSC, which indicates that the mix acid treatment enhances the adsorption capacity of biochar.

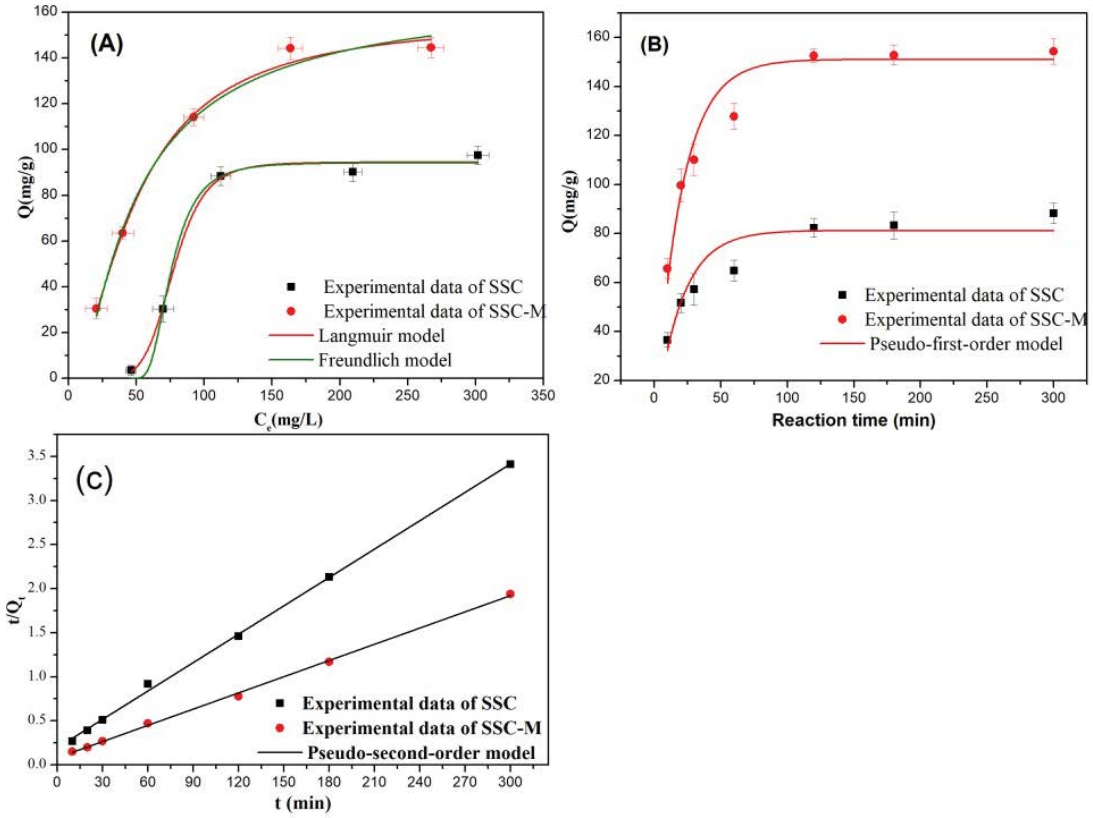

Fig. 7. Influence of experimental parameters on Pb(II) adsorption by SSC and SSC-M: (A) effect of equilibrium Pb(II) concentration, where pH = 5.0; m/v = 1 g L^{-1}; t = 120 min, (B) effect of different contact times, where C_0[Pb(II)] = 200 mg L^{-1}; pH = 5.0; m/v = 1 g L^{-1}; t = 120 min and (C) pseudo-second-order models for adsorption of Pb(II) onto SSC and SSC-M.

3.2.3. Effect of adsorption time

The effect of contact time on the adsorption of Pb(II) by biochar was also investigated. As shown in Fig. 7B, the adsorption of Pb(II) onto both adsorbents increased with time and attained equilibrium within 2 h. Further, an increase in contact time did not result in an increase in adsorption. This may indicate that an adsorption equilibrium is achieved owing to the saturation of the adsorbent's active sites. The initial quick rate of adsorption can be attributed to unoccupied adsorptive sites as well as the driving force from large concentration gradients [37]. As free active sites become gradually occupied and the repulsive force enhances on the solid–liquid interface, the adsorption rate decreases and reaches equilibrium.

3.3. Adsorption analysis

3.3.1. Adsorption isotherms

The adsorption isotherm is an important index for understanding the process of biochar adsorption of metal ions. Therefore, to further examine the Pb(II) adsorption characteristics of SSC and SSC-M, adsorption isotherm analyses were performed on both biochars under equilibrium conditions, and the adsorption isotherm curves were fitted by the Langmuir and Freundlich models. The fitting curves are depicted in Fig. 7A and the model parameters obtained from non-linear regression analysis are presented in Table 3. The Langmuir model assumes homogeneous adsorption where adsorption sites on a uniform surface have equivalent adsorbate affinity and monolayer adsorption [38]. In comparison, the Freundlich model assumes [39] that the adsorbent surface is heterogeneous and characterises multilayer and non-ideal adsorption on the heterogeneous surface. From Table 3, it was observed that the Langmuir isotherm model has a higher correlation coefficient (R^2) and is lower in SD, RMSE, and RSSE when compared to the Freundlich model. Thus the adsorption process of Pb(II) onto SSC and SSC-M follows the Langmuir isotherm model, indicating monolayer adsorption sites with homogeneous nature of the adsorbent without any interaction between adsorbed molecules. Additionally, parameter b that is related to the affinity of the binding sites allows the comparison of the sorbent affinities towards the Pb(II) [40]. The adsorption affinity of SSC-M was stronger than that of SSC. The maximum Pb(II) adsorption capacity of SSC-M calculated by the Langmuir model was 156.05 mg g^{-1}, which is obviously greater than that of the adsorbent reported in previous researches (Table 4).

3.3.2. Adsorption kinetics

The pseudo-first-order kinetic equation (PFO) and the pseudo-second-order kinetic equation (PSO) can explain the biochar adsorption mechanism for Pb(II) from the model point of view [48–51]. PFO assumes that the adsorption occurs entirely via physisorption, [52] whereas PSO is based on chemisorption that involves electron exchange between adsorbate and adsorbent [37]. Kinetic studies of Pb(II) sorption processes from a single-component system with the two biochars pointed to 2-phase processes occurring in the initial rapid sorption during the first 0.5 h followed by a slower uptake until the sorption equilibrium is reached in 2 h. The first step can be attributed to the rapid occupation of easily accessible external surface sorption sites. Residual sites with lower affinities are occupied slowly, and this phase corresponds to the formation of inner layer complexes or slow diffusion into the pores. The fitting curves of these models were plotted in Fig. 7B and C and kinetic parameters obtained by the non-linear regression analysis are shown in Table 5. Experimental data of the two biochars are fitted well to the PSO kinetic equation ($R^2 > 0.999$), implying that the rate-controlling mechanism for the adsorption of Pb(II) on the biochars is by chemical adsorption involving covalent forces through sharing or exchanging of electrons between the adsorbent and adsorbate [53].

3.4. Reusability of biochar adsorbents

The reusability experiments aimed at reducing the running cost and test the regenerability of the modified

Table 3
Isotherm constants for the adsorption of Pb(II) onto SSC and SSC-M using nonlinear models

Isotherm model	Parameters	Values for SSC	Values for SSC-M
Langmuir	q_m	94.16	156.48
	b	0.274	0.213
	R^2	0.995	0.992
	SD	0.1104	0.02515
	RSSE	29.7644	50.4108
	RMSE	2.4398	3.1752
Freundlich	K_F	94.51	167.39
	$1/n$	0.128	0.122
	R^2	0.989	0.987
	SD	0.4997	0.04568
	RSSE	38.7392	84.3915
	RMSE	2.7835	4.1083

Table 4
Pb(II) adsorption capacity of different adsorbents

Absorbate	Modified reagent	T (°C)	Adsorption capacity Q (mg g^{-1})	Reference
Palm	β-cyclodextrin	500	90.30	[15]
Rice straw	β-cyclodextrin	500	130.60	
Coconut shell	Phosphoric acid	600	49.92	[24]
Camellia seed husk	/	700	109.67	[33]
Cotton straw	/	600	124.70	[41]
Waste chicken feathers	KOH	450	119.65	[42]
Watermelon seeds	H_2O_2	350	60.87	[43]
Sludge	KOH	700	57.48	[44]
Corn stalk	/	450	49.70	[45]
Sewage sludge	/	500	116.2	[46]
Sewage sludge digestate	KOH	350	106	[47]
Sewage sludge digestate	H_2O_2	350	90	[47]
Shrimp shells	/	800	94.49	this study
	HNO_3–H_2SO_4	800	156.05	

Table 5
Kinetic model parameters for adsorption of Pb(II) onto SSC and SSC-M

Kinetic model	Parameters	Values for SSC	Values for SSC-M
Pseudo-first-order	q_e (mg g^{-1})	81.22	151.08
	k_1 (min^{-1})	0.050	0.051
	R^2	0.893	0.959
	SD	0.10787	0.07222
	RMSE	271.3566	376.6347
	RSSE	6.2262	7.3352
Pseudo-second-order	q_e (mg g^{-1})	90.9	166.67
	k_2 (g mg^{-1} min^{-1})	0.062	0.045
	R^2	0.999	0.999
	SD	0.06222	0.04340
	RMSE	70.8211	119.7140
	RSSE	3.1808	4.1355

biochar [6]. Recent studies utilized HNO_3 or HCl solution as an effective eluent for the regeneration of adsorbents, having a reversible exchange mechanism between metal ions and the adsorbent [54]. In the current study, HCl at pH = 1.0 was used as eluent for the regeneration process of both SSC and SSC-M, and the regeneration process was evaluated by five consecutive cycles of repeated adsorption (Fig. 8). After these five consecutive cycles, SSC-M showed a consistent higher adsorption efficiency towards Pb(II), the adsorption capacity of Pb(II) decreased from 75.70% to 50.67%. A slight decrease was observed, which could be ascribed to the incomplete desorption of Pb(II) onto the surface of the adsorbents, and also due to the solid loss in the solution [43]. It demonstrated that there were some attractive sites that could not be completely reversed during the desorption process [55]. Although the adsorption capacity of biochar declined with recycling time, the Pb(II) removal efficiency was higher than 50% after 5 successive recycles, suggesting that shrimp shells-based biochar modified by mixed acid had high reusability and was a promising adsorbent for the Pb(II) removal.

3.5. SSC-M adsorption mechanism for Pb(II)

Analysis of adsorption kinetics and isotherms showed that chemical adsorption on the monolayer surfaces played a dominant role in the SSC-M removal of Pb(II) from water. The microstructure and functional groups of biochar were analysed by a series of characterisations to further study the mechanism of Pb(II) adsorption by SSC-M. The possible structure of the SSC-M surface can be approximated using these characterisations, as shown in Fig. 9.

After modification, the specific surface area of biochar decreased from 291.3 to 178.14 m^2 g^{-1}, whereas the adsorption capacity and removal rate of SSC-M with respect to Pb(II) was higher than that of SSC. Thus, it is not true that the larger the specific area, the better the adsorption effect [56]. SEM and FTIR results showed that the surface structure

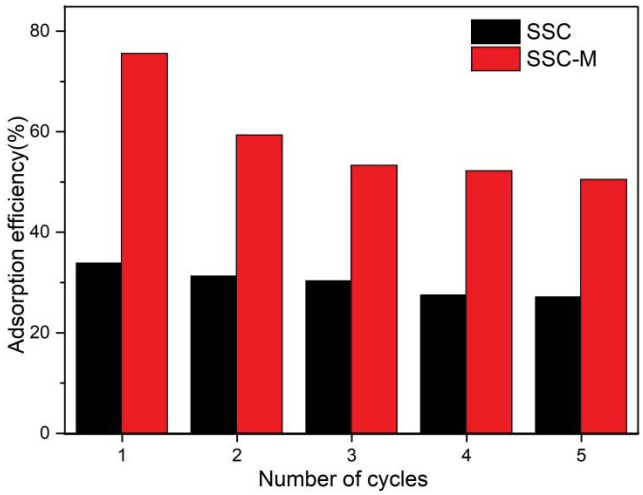

Fig. 8. Effect of regeneration times on adsorption efficiency.

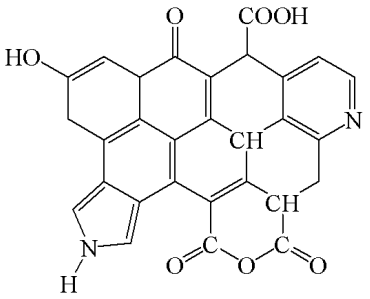

Fig. 9. The ideal structural diagram of SSC-M.

and chemical properties of biochar were changed to an extent by modification. The layered structure of modified biochar was observed to be more complex, and the pore structure also changed from a uniform size to slits. These changes can significantly increase the contact area between the biochar surface and adsorbates, which is conducive to the diffusion of adsorbates on the surface of carbon materials.

As seen in Fig. 1C, the pH_{PZC} of SSC was 2.37, whereas the pH_{PZC} of SSC-M was reduced to 2.29. It had been established earlier that increasing the pH decreases the protonation of the functional groups on the adsorbent surface and, therefore, enhances Pb(II) adsorption via electrostatic attractions. The specific electrostatic interactions of SSC-M adsorption of Pb(II) on SSC-M are shown in Fig. 10.

The surface of SSC-M contains carboxyl and hydroxyl groups, according to the FTIR analysis. The hydroxyl and carboxyl groups at the surface can exchange a proton with positively charged Pb(II) species in the aqueous solution to form an ion-exchange complex. The ion exchange mechanism between H+ on the adsorbent surface and the metal ion can be described by the following reactions:

$$2\left(C-COOH\right)+Pb^{2+}\rightarrow\left(C-COO\right)_2Pb+2H^{+} \quad (9)$$

$$2\left(C-OH\right)+Pb^{2+}\rightarrow\left(C-O\right)_2Pb+2H^{+} \quad (10)$$

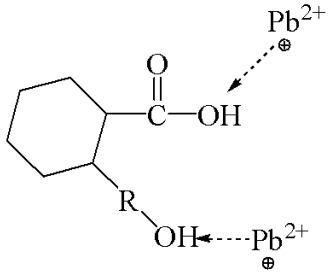

Fig. 10. Schematic diagram of SSC-M adsorption of Pb^{2+} by electrostatic interaction.

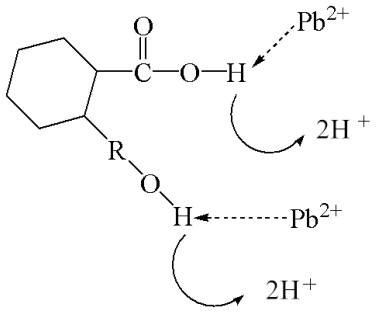

Fig. 11. Schematic of adsorption of Pb(II) by surface complexation.

The specific adsorption is shown in Fig. 11.

This process can be confirmed by the following: the pH of the solution before SSC-M adsorbs Pb(II) is 5.0, and the pH of the solution after Pb(II) adsorption is 3.2. This indicates that the pH of the solution after Pb(II) adsorption decreases, which confirms the release of H^+ ions into the solution, as shown in the ion exchange in Eqs. (2) and (3).

4. Conclusion

The mixed-acid-modified and shrimp shell-derived biochar (SSC-M) showed a significant adsorption capacity for Pb(II). The modification reduced the pH_{PZC} of biochar from 2.37 to 2.29, which increased the electrostatic interactions between adsorbents and Pb(II); however, the modification also ensured that the biochar was loaded with more oxygen-containing functional groups such as carboxyl groups which have surface complexation with Pb. The equilibrium adsorption data indicated best fit to the Langmuir isotherm model and the maximum monolayer adsorption capacity, q_{max}, was found to be 156.48 mg g^{-1}. It was found that the kinetic adsorption follows very well the pseudo-second-order model, indicating the chemisorption. The SSC-M biochar in this study acts as a novel alternative for removing Pb(II) from aqueous solutions, and simultaneously promotes biowaste utilisation and sustainable waste management. However, further studies are still needed to develop new low-cost and high-efficiency modification technologies for biochar, and to increase the practical application of these resulting sorbents in wastewater treatment. For industrial application,

the preparation conditions of biochar need to be further improved based on the different environmental purposes.

Acknowledgments

This work was supported by the Technology Innovation Special Foundation of Hubei Province (2019ACA152 and 2020ZYYD019).

References

[1] J.-M. Wang, J. Zhao, X.-Z. Qin, Z. Wang, Theoretical study of adsorption mechanism of heavy metals As and Pb on the calcite (104) surface, Mater. Today Commun., 104 (2020) 101742, doi: 10.1016/j.mtcomm.2020.101742.
[2] Z.Y. Wu, X.X. Chen, B.L. Yuan, M.-L. Fu, A facile foaming-polymerization strategy to prepare 3D MnO_2 modified biochar-based porous hydrogels for efficient removal of Cd(II) and Pb(II), Chemosphere, 239 (2020) 124745, doi: 10.1016/j.chemosphere.2019.124745.
[3] Ministry of Health of the People's Republic of China, Standards for Drinking Water Quality, GB5749-2006, 2006.
[4] X. Hu, L.J. Jia, J. Cheng, Z.R. Sun, Magnetic ordered mesoporous carbon materials for adsorption of minocycline from aqueous solution: preparation, characterization and adsorption mechanism, J. Hazard. Mater., 362 (2019) 1–8.
[5] L. Long, Y.W. Xue, X.L. Hu, Y. Zhu, Study on the influence of surface potential on the nitrate adsorption capacity of metal modified biochar, Environ. Sci. Pollut. Res., 26 (2019) 3065–3074.
[6] N. Li, M.L. Yin, D.C.W. Tsang, S.T. Yang, J. Liu, X. Li, G. Song, J. Wang, Mechanisms of U(VI) removal by biochar derived from *Ficus microcarpa* aerial root: a comparison between raw and modified biochar, Sci. Total Environ., 697 (2019) 134115, doi: 10.1016/j.scitotenv.2019.134115.
[7] X.X. Huang, Y.G. Liu, S.B. Liu, X.F. Tan, Y. Ding, G.M. Zeng, Y.Y. Zhou, M.M. Zhang, S.F. Wang, B.H. Zheng, Effective removal of Cr(VI) using β-cyclodextrin-chitosan modified biochars with adsorption/reduction bifuctional roles, RSC Adv., 6 (2016) 94–104.
[8] M.-M. Zhang, Y.-G. Liu, T.-T. Li, W.-H. Xu, B.-H. Zheng, X.-F. Tan, H. Wang, Y.-M. Guo, F.-Y. Guo, S.-F. Wang, Chitosan modification of magnetic biochar produced from *Eichhornia crassipes* for enhanced sorption of Cr(VI) from aqueous solution, RSC Adv., 5 (2015) 46955–46964.
[9] E. Altıntıg, H. Altundag, M. Tuzen, A. Sarı, Effective removal of methylene blue from aqueous solutions using magnetic loaded activated carbon as novel adsorbent, Chem. Eng. Res. Des., 122 (2017) 151–163.
[10] T.A. Saleh, M. Tuzen, A. Sarı, Magnetic activated carbon loaded with tungsten oxide nanoparticles for aluminum removal from waters, J. Environ. Chem. Eng., 5 (2017) 2853–2860.
[11] T.A. Saleh, A. Sarı, M. Tuzen, Effective adsorption of antimony(III) from aqueous solutions by polyamide-graphene composite as a novel adsorbent, Chem. Eng. J., 307 (2017) 230–238.
[12] Y.Q. Sun, I.K.M. Yu, D.C.W. Tsang, X.D. Cao, D.H. Lin, L.L. Wang, N.J.D. Graham, D.S. Alessi, M. Komárek, Y.S. Ok, Y.J. Feng, X.-D. Li, Multifunctional iron-biochar composites for the removal of potentially toxic elements, inherent cations, and hetero-chloride from hydraulic fracturing wastewater, Environ. Int., 124 (2019) 521–532.
[13] X.Y. Lu, W.L. Yim, B.H.R. Suryanto, C. Zhao, Electrocatalytic oxygen evolution at surface-oxidized multiwall carbon nanotubes, J. Am. Chem. Soc., 137 (2015) 2901–2907.
[14] Y.Y. Deng, S. Huang, D.A. Laird, X.G. Wang, Z.W. Meng, Adsorption behaviour and mechanisms of cadmium and nickel on rice straw biochars in single- and binary-metal systems, Chemosphere, 218 (2019) 308–318.
[15] H.-T. Zhao, S. Ma, S.-Y. Zheng, S.-W. Han, F.-X. Yao, X.-Z. Wang, S.-S. Wang, K. Feng, β-cyclodextrin functionalized biochars as novel sorbents for high-performance of Pb^{2+} removal, J. Hazard. Mater., 362 (2019) 206–213.
[16] A.K. Mondal, K. Kretschmer, Y.F. Zhao, H. Liu, H.B. Fan, G.X. Wang, Naturally nitrogen doped porous carbon derived from waste shrimp shells for high-performance lithium ion batteries and supercapacitors, Microporous Mesoporous Mater., 246 (2017) 72–80.
[17] G.Q. Yuan, Y.X. Pan, W.W. Li, C. Wang, H.X. Chen, Effect of extrusion on physicochemical properties, functional properties and antioxidant activities of shrimp shell wastes protein, Int. J. Biol. Macromol., 136 (2019) 1096–1105.
[18] R.J. White, M. Antonietti, M.-M. Titirici, Naturally inspired nitrogen doped porous carbon, J. Mater. Chem., 19 (2009) 8645–8650.
[19] S.S. Pattanaik, P.B. Sawant, K.A. Martin Xavier, K. Dube, P. Prakash Srivastava V. Dhanabalan, N.K. Chadha, Characterization of carotenoprotein from different shrimp shell waste for possible use as supplementary nutritive feed ingredient in animal diets, Aquaculture, 515 (2020) 734594, doi: 10.1016/j.aquaculture.2019.734594.
[20] C. He, H.L. Lin, L.L. Dai, R.L. Qiu, Y.T. Tang, Y.P. Wang, P.-G. Duan, Y.S. Ok, Waste shrimp shell-derived hydrochar as an emergent material for methyl orange removal in aqueous solutions, Environ. Int., 134 (2020) 105340, doi: 10.1016/j.envint.2019.105340.
[21] L. Qin, Z.P. Zhou, J.D. Dai, P. Ma, H.B. Zhao, J.S. He, A. Xie, C.X. Li, Y.S. Yan, Novel N-doped hierarchically porous carbons derived from sustainable shrimp shell for high-performance removal of sulfamethazine and chloramphenicol, J. Taiwan Inst. Chem. Eng., 62 (2016) 228–238.
[22] J.-H. Park, J.J. Wang, R. Xiao, B.Y. Zhou, R.D. Delaune, D.-C. Seo, Effect of pyrolysis temperature on phosphate adsorption characteristics and mechanisms of crawfish char, J. Colloid Interface Sci., 525 (2018) 143–151.
[23] S. Brunauer, L.S. Deming, W.E. Deming, E. Teller, On a theory of the van der Waals adsorption of gases, J. Am. Chem. Soc., 62 (1940) 1723–1732.
[24] G.E. Sharaf El-Deen, S.E.A. Sharaf El-Deen, Kinetic and isotherm studies for adsorption of Pb(II) from aqueous solution onto coconut shell activated carbon, Desal. Water Treat., 57 (2016) 1944–3994.
[25] F. Rouquerol, J. Rouquerol, K. Sing, Adsorption by Powders and Porous Solids, Academic Press, New York, 1999.
[26] J.Q. Deng, Y.G. Liu, S.B. Liu, G.M. Zeng, X.F. Tan, B.Y. Huang, X.J. Tang, S.F. Wang, W. Hua, Z.L. Yan, Competitive adsorption of Pb(II), Cd(II) and Cu(II) onto chitosan-pyromellitic dianhydride modified biochar, J. Colloid Interface Sci., 506 (2017) 355–364.
[27] S.T. Xing, C. Hu, J.H. Qu, H. He, M. Yang, Characterization and reactivity of MnO_x supported on mesoporous zirconia for herbicide 2,4-D mineralization with ozone, Environ. Sci. Technol., 42 (2008) 3363–3368.
[28] Z.G. Song, F. Lian, Z.H. Yu, L.Y. Zhu, B.S. Xing, W.W. Qiu, Synthesis and characterization of a novel MnO_x-loaded biochar and its adsorption properties for Cu^{2+} in aqueous solution, Chem. Eng. J., 242 (2014) 36–42.
[29] P.K. Godwin, Y.F. Pan, H.N. Xiao, M.F. Afzal, Progress in preparation and application of modified biochar for improving heavy metal ion removal from wastewater, J. Bioresour. Bioprod., 4 (2016) 31–42.
[30] W.J. Zhu, Y.G. Zhang, P.L. Wang, Z.Y. Yang, A. Yasin, L.T. Zhang, Preparation and applications of salt-resistant superabsorbent poly(acrylic acid-acrylamide/fly ash) composite, Materials, 12 (2019) 596, doi: 10.3390/ma12040596.
[31] C. Lai, M.M. Zhang, B.S. Li, D.L. Huang, G.M. Zeng, L. Qin, X.G. Liu, H. Yi, M. Cheng, L. Li, Z. Chen, L. Chen, Fabrication of CuS/$BiVO_4$ (0 4 0) binary heterojunction photocatalysts with enhanced photocatalytic activity for Ciprofloxacin degradation and mechanism insight, Chem. Eng. J., 358 (2019) 891–902.
[32] L.-L. Ling, W.-J. Liu, S. Zhang, H. Jiang, Magnesium oxide embedded nitrogen self-doped biochar composites: fast and

high-efficiency adsorption of heavy metals in an aqueous solution, Environ. Sci. Technol., 51 (2017) 10081–10089.
[33] J.W. Wu, T. Wang, Y.S. Zhang, W.-P. Pan, The distribution of Pb(II)/Cd(II) adsorption mechanisms on biochars from aqueous solution: considering the increased oxygen functional groups by HCl treatment, Bioresour. Technol., 291 (2019) 121859, doi: 10.1016/j.biortech.2019.121859.
[34] M.I. Inyang, B. Gao, Y. Yao, Y.W. Xue, A. Zimmerman, A. Mosa, P. Pullammanappallil, Y.S. Ok, X.D. Cao, A review of biochar as a low-cost adsorbent for aqueous heavy metal removal, Crit. Rev. Env. Sci. Technol., 46 (2016) 406–433.
[35] Q. An, Y.-Q. Jiang, H.-Y. Nan, Y. Yu, J.-N. Jiang, Unraveling sorption of nickel from aqueous solution by $KMnO_4$ and KOH-modified peanut shell biochar: implicit mechanism, Chemosphere, 214 (2019) 846–854.
[36] H.-C. Tao, H.-R. Zhang, J.-B. Li, W.-Y. Ding, Biomass based activated carbon obtained from sludge and sugarcane bagasse for removing lead ion from wastewater, Bioresour. Technol., 192 (2015) 611–617.
[37] W. Zhang, Q. Deng, Q.L. He, J.Y. Song, S.L. Zhang, H.Y. Wang, J.P. Zhou, H.N. Zhang, A facile synthesis of core-shell/bead-like poly (vinyl alcohol)/alginate@PAM with good adsorption capacity, high adaptability and stability towards Cu(II) removal, Chem. Eng. J., 351 (2018) 462–472.
[38] H.M.F. Freundlich, Over the adsorption in solution, J. Phys. Chem., 57 (1906) 385–471.
[39] I. Langmuir, The adsorption of gases on plane surfaces of glass, mica and platinum, J. Am. Chem. Soc., 40 (1918) 1361–1403.
[40] A. Krajňák, L. Pivarčiová, O. Rosskopfová, M. Galamboš, P. Rajec, Adsorption of nickel on rhyolitic Slovak bentonites, J. Radioanal. Nucl. Chem., 304 (2015) 587–593.
[41] Z.Z. Wang, J. Xu, D. Yellezuome, R.H. Liu, Effects of cotton straw-derived biochar under different pyrolysis conditions on Pb(II) adsorption properties in aqueous solutions, J. Anal. Appl. Pyrolysis, 157 (2021) 105214, doi: 10.1016/j.jaap.2021.105214.
[42] H.Y. Chen, X.J. Yang, Y.L. Liu, X.M. Lin, J.J. Wang, Z. Zhang, N. Li, Y.T. Li, Y.L. Zhang, KOH modification effectively enhances the Cd and Pb adsorption performance of N-enriched biochar derived from waste chicken feathers, Waste Manage., 130 (2021) 82–92.
[43] W. Ahmed, S. Mehmood, A. Núñez-Delgado, A. Ali, M. Qaswar, A. Shakoor, M. Mahmood, D.-Y. Chen, Enhanced adsorption of aqueous Pb(II) by modified biochar produced through pyrolysis of watermelon seeds, Sci. Total Environ., 784 (2021) 147136, doi: 10.1016/j.scitotenv.2021.147136.
[44] J.J. Zhang, J.G. Shao, Q.Z. Jin, Z.Q. Li, X. Zhang, Y.Q. Chen, S.H. Zhang, H.P. Chen, Sludge-based biochar activation to enhance Pb(II) adsorption, Fuel, 252 (2019) 101–108.
[45] L.Q. Liu, Y.J. Huang, S.P. Zhang, Y. Gong, Y.H. Su, J.H. Cao, H.J. Hu, Adsorption characteristics and mechanism of Pb(II) by agricultural waste-derived biochars produced from a pilot-scale pyrolysis system, Waste Manage., 100 (2019) 287–295.
[46] Y.J. Xue, C. Wang, Z.H. Hu, Y. Zhou, Y. Xiao, T. Wang, Pyrolysis of sewage sludge by electromagnetic induction: biochar properties and application in adsorption removal of Pb(II), Cd(II) from aqueous solution, Waste Manage., 89 (2019) 48–56.
[47] S. Wongrod, S. Simon, G. Guibaud, P.N.L. Lens, Y. Pechaud, D. Huguenot, E.D. van Hullebusch, Lead sorption by biochar produced from digestates: Consequences of chemical modification and washing, J. Environ. Manage., 219 (2018) 277–284.
[48] J.O. Eniola, R. Kumar, A.A. Al-Rashdi, M.A. Barakat, Hydrothermal synthesis of structurally variable binary CuAl, MnAl and ternary CuMnAl hydroxides for oxytetracycline antibiotic adsorption, J. Environ. Chem. Eng., 8 (2019) 103535, doi: 10.1016/j.jece.2019.103535.
[49] S. Lagergren, About the theory of so-called adsorption of soluble substances, Kungliga Svenska Vetenskapsakademiens, Handlingar, 24 (1898) 1–39.
[50] J.-P. Simonin, On the comparison of pseudo-first-order and pseudo-second-order rate laws in the modeling of adsorption kinetics, Chem. Eng. J., 300 (2016) 254–263.
[51] H.N. Tran, S.-J. You, A. Hosseini-Bandegharaei, H.-P. Chao, Mistakes and inconsistencies regarding adsorption of contaminants from aqueous solutions: a critical review, Water Res., 120 (2017) 88–116.
[52] L. Sun, S.G. Wan, W.S. Luo, Biochars prepared from anaerobic digestion residue, palm bark, and eucalyptus for adsorption of cationic methylene blue dye: characterization, equilibrium, and kinetic studies, Bioresour. Technol., 140 (2013) 406–413.
[53] J.T. Liu, X. Ge, X.X. Ye, G.Z. Wang, H.M. Zhang, H.J. Zhou, Y.X. Zhang, H.J. Zhao, 3D graphene/δ-MnO_2 aerogels for highly efficient and reversible removal of heavy metal ions, J. Mater. Chem., 4 (2016) 1970–1979.
[54] H.S. Li, X.W. Li, T.F. Xiao, Y.H. Chen, J.Y. Long, G.S. Zhang, P. Zhang, C.L. Li, L.Z. Zhuang, K. Li, Efficient removal of thallium(I) from wastewater using flower-like manganese dioxide coated magnetic pyrite cinder, Chem. Eng. J., 353 (2018) 867–877.
[55] Q. Yang, X.L. Wang, W. Luo, J. Sun, Q.X. Xu, F. Chen, J.W. Zhao, S. Wang, F.B. Yao, D.B. Wang, X.M. Li, G.M. Zeng, Effectiveness and mechanisms of phosphate adsorption on iron-modified biochars derived from waste activated sludge, Bioresour. Technol., 247 (2018) 537–544.
[56] M.C. Zhang, A.M. Li, Q. Zhou, C.D. Shuang, W.W. Zhou, M.Q. Wang, Effect of pore size distribution on tetracycline adsorption using magnetic hypercrosslinked resins, Microporous Mesoporous Mater., 184 (2014) 105–111.